J. Fluid Mech. (1984), *vol.* 144, *pp.* 363–387
Printed in Great Britain

The interference of thermal fields from line sources in grid turbulence

By Z. WARHAFT

Sibley School of Mechanical and Aerospace Engineering, Cornell University, Ithaca, NY 14853

(Received 2 August 1983 and in revised form 19 December 1983)

The interference of passive thermal fields produced by two (and more) line sources in decaying grid turbulence is studied by using the inference method described by Warhaft (1981) to determine the cross-correlation coefficient ρ between the temperature fluctuations produced by the sources. The evolution of ρ as a function of downstream distance, for $0.075 < d/l < 10$, where d is the wire spacing and l is the integral lengthscale of the turbulence, is determined for a pair of sources located at various distances from the grid. It is found that ρ may be positive or negative (thereby enhancing or diminishing the total temperature variance) depending on the line-source spacing, their location from the grid and the position of measurement. It is also shown that the effects of a mandoline (Warhaft & Lumley 1978) may be idealized as the interference of thermal fields produced by a number of line sources. Thus new light is shed on the rate of decay of scalar-variance dissipation. The thermal field of a single line source is also examined in detail, and these results are compared with other recent measurements.

1. Introduction

Despite the desirability of being able to predict how a passive scalar contaminant such as heat, moisture or chemical species is transported and mixed in a turbulent flow field, the problem still remains unsolved from a fundamental viewpoint, even if the turbulent field is completely specified. The difficulty stems in part from the way the scalar is introduced into the flow; in any realistic problem the scalar field is initiated (be it from a point or a distributed source) at a scale vastly different from that of the turbulence.

One of the simplest ways of injecting a scalar into a turbulent field is by means of placing a fine heated wire in the flow. If the wire is fine enough and if the wire overheat is small enough neither the wire's physical presence nor the resultant thermal wake will change the background velocity field, i.e. the resultant scalar field will be a passive contaminant. The first detailed theoretical study of this problem appears to have been done by Taylor (1935) (see also Taylor 1921), yet after nearly fifty years of research, accurate theoretical understanding of how the mean and variance (not to mention higher-order moments) of the thermal field evolves has not been achieved (for a summary of previous theoretical and experimental work on this subject see Hinze 1975). Very recently, however, such theoretical tools as two-particle dispersion theory (Durbin 1980; Lundgren 1981; Sawford 1983; Sawford & Hunt 1983) and the joint probability density function (p.d.f.) approach (Anand & Pope 1983) have shed new light on this problem. Important experiments concerning the spreading rate of both the mean and fluctuating thermal field for a line source have been carried out by Uberoi & Corrsin (1953) and by Townsend (1954), although

information on how the thermal field behaves very close to the source has only been obtained recently (Stapountzis *et al.* 1984).

The superposition of two or more passive thermal wakes downstream of parallel line sources is an important and non-trivial extension of the case of a single source. The way these line sources mix will be a function of their spacing and the lengthscale and intensity of the turbulence. Experimental knowledge of this mixing is important in testing two-particle dispersion theories. Furthermore, a study of the superposition of multiple line sources should provide deeper insight into the problem of scalar variance dissipation: the mandoline used by Warhaft & Lumley (1978) consists of an array of parallel wires, and the non-unique value of the scalar dissipation rate observed in that study was due to variations in the spacing (and downstream location from the grid) of the mandoline wires. Knowledge of the superposition of multiple sources also has practical application in such diverse areas as heat exchangers, the feeding of chemical reactants into a turbulent mixer, the mixing of multiple plumes from industrial effluent, and mixing (of CO_2 or O_2) above plant or crop canopies.

If we consider two line sources located in a turbulent flow (decaying grid turbulence for the situation to be studied here) the resultant temperature variance will be

$$\overline{\theta_B^2} = \overline{(\theta_1+\theta_2)^2} = \overline{\theta_1^2}+\overline{\theta_2^2}+2\rho\,(\overline{\theta_1^2})^{\frac{1}{2}}\,(\overline{\theta_2^2})^{\frac{1}{2}}, \tag{1}$$

where θ_1 and θ_2 are the thermal fluctuations produced by each wire and ρ is the cross-correlation coefficient between the fluctuations produced by each wire. Warhaft (1981) has shown (for two distributed line sources) that ρ may be inferred by operating each thermal source separately (thus determining $\overline{\theta_1^2}$ and $\overline{\theta_2^2}$) and then both together (determining $\overline{\theta_B^2}$). Equation (1) may then be solved for ρ. Here this inference method is used to study the interference of two parallel line sources placed in a plane, parallel to and downstream from the grid (figure 1).†

Equation (1) can also be extended to examine the interference of multiple line sources. Here the relation for the temperature variance is

$$\overline{\theta_T^2} = \overline{\theta_1^2}+\overline{\theta_2^2}\ldots+2\rho_{12}\,(\overline{\theta_1^2})^{\frac{1}{2}}\,(\overline{\theta_2^2})^{\frac{1}{2}}+2\rho_{13}\,(\overline{\theta_1^2})^{\frac{1}{2}}\,(\overline{\theta_3^2})^{\frac{1}{2}}+\ldots. \tag{2}$$

Equation (2) shows that for a mandoline (a parallel array of heated wires evenly spaced across the tunnel) the evolution of the temperature variance is solely a function of the temperature variance of each wire and ρ_{ab}. The interference of multiple line sources is also described here.

The outline of the paper is as follows. First, the evolution of the mean and variance of the thermal field downstream of a single line source is examined. These results supplement the recent work of Stapountzis *et al.* (1984), although here the distance

† We use the term *interference* for the variance field (equation 1) in the same sense that it is used in linear wave theory where destructive or constructive interference may occur depending on the phase relation of the two superposed waves. The cross-correlation coefficient ρ in equation (1) may be positive or negative, thereby enhancing the value of $\overline{\theta_B^2}$ (constructive interference) or reducing it (destructive interference). Of course no mechanical interference occurs, since the thermal fields are passive and the line sources do not affect the velocity field. Frequently throughout this paper we will use the expression 'interference of line sources'; it should be understood to be the interference of the thermal fields produced by the line sources that is being addressed. Note also that the equation for the total (mean-squared) temperature field is

$$\overline{[(T_1+\theta_1)+(T_2+\theta_2)]^2} = T_1^2+T_2^2+2T_1T_2+\overline{\theta_1^2}+\overline{\theta_2^2}+2\overline{\theta_1\theta_2}, \tag{1'}$$

where T is the mean temperature. Information concerning the first five terms on the right-hand side of (1′) could be obtained from one wire only. It is the final term, the covariance of the temperature fluctuations (and its associated cross-correlation coefficient $\rho \equiv \overline{\theta_1\theta_2}/(\overline{\theta_1^2})^{\frac{1}{2}}\,(\overline{\theta_2^2})^{\frac{1}{2}}$) that is of singular importance in the interference process.

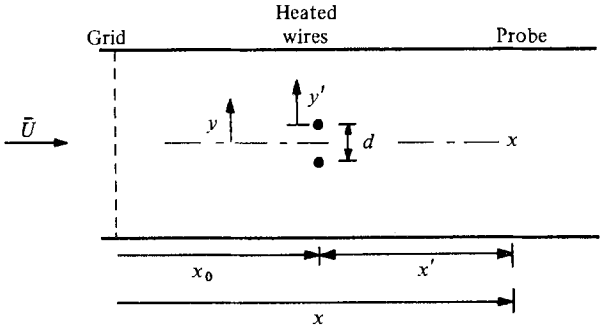

FIGURE 1. Sketch of wind tunnel showing two heated wires. When two or more heated wires are used the transverse direction y (through which the probe is moved) is measured from the midpoint between the two central wires. For experiments with one wire only (figures 4 to 12) the transverse direction y' is measured from the wire itself.

of the line source from the grid is varied and new results are also described for the thermal field very far downstream from the source. Secondly, extensive measurements of the interference of two line sources are presented. For this experiment the distance of the sources from the grid (x_0, figure 1) and the wire spacing d are varied in a systematic way. Thirdly, experiments on the interference of multiple line sources are described, and these results are discussed in terms of the previous mandoline experiments of Warhaft & Lumley (1978). Although the present approach appears to be new, an interesting experiment by Kistler (1954) bears some relation to the work described here. In that experiment Kistler studied the joint p.d.f. of two line sources in grid turbulence; however, the inference method, which is the basis of the work to be described here, was not employed to determine the correlation between the two sources.

2. Apparatus

The open-circuit wind tunnel was the same as that used in our previous studies (Warhaft 1981; Sirivat & Warhaft 1983). The mesh length M of the biplane turbulence-generating grid was 0.025 m and the grid bars were 0.476 cm square-sectioned, giving a grid solidity of 0.34. The tunnel test section was $170M$ long and $16M \times 16M$ in cross-section. The walls of the tunnel were slightly divergent to ensure a constant centreline mean speed with the development of the boundary layer. The mean wind speed was 7 m/s for all experiments to be described here.

The thermal line sources were nichrome wires of 0.127 mm diameter (and for some experiments 0.207 mm diameter). Thus the (cold) wire Reynolds number Re was 57 (and sometimes 91). Note that, when the wires are heated, Re, based on the viscosity of the air film surrounding the wire, is considerably reduced. However, close to the source some disturbance to the velocity field due to these wires was observed. Hence for the study of the thermal field $\leqslant 8M$ from the source, 0.025 mm diameter platinum wire was used. Low heating current (100 mA) was also used so as not to affect the flow field by thermal means near to the wire. For this case the cold wire Re was 11. For x'/M greater than about 10, where x' is the distance from the thermal source (placed at x_0) (figure 1) it will be shown below that the thermal-variance evolution is independent of the wire diameter for (at least) the Reynolds-number range 39–280. Small springs were placed in tension between the ends of the thicker

(0.127 mm and 0.207 mm) wires and the tunnel wall in order to prevent sagging when these wires were heated. For the fine (0.025 mm) wire, sagging was prevented by placing small weights on each end of the wire after it had been threaded through small holes in the tunnel wall.

The mean temperature was measured by a 7.62×10^{-5} m diameter chromal–constantan thermocouple. In order to compensate for variations in room temperature, the reference of the thermocouple was placed in the wind tunnel but well away from the thermal field produced by the line source. Thus effects of variation in background temperature were subtracted out. Temperature fluctuations were measured with a 1.27 μm platinum wire with length-to-diameter ratio $L/D = 400$ for the etched portion of the wire. The total length of the wire was $3L$, thus alleviating much of the probe prong–wire interaction effect recently described by Paranthoen, Petit & Lecordier (1982). The fast-response a.c. temperature bridge was the same as that used by Warhaft & Lumley (1978). Particular care was taken to align the sensing wires of the thermocouple and fast response resistance thermometer parallel to the heated line source when measuring close to the source in order to avoid resolution problems. Measurements of temperature fluctuations in the 'cold' flow revealed that the r.m.s. noise level (combined electrical and tunnel) was approximately 5×10^{-3} °C. The temperature variance measurements were corrected for this noise under the assumption of zero correlation between the signal and noise fluctuations. Velocity fluctuations were measured by means of DISA type 55M constant-temperature bridges. The u (longitudinal velocity) and v (lateral velocity) components were measured with a 90° X-wire array, $L/D = 200$. The wires were 3.1 μm tungsten and the wire overheat was 1.8. Some confirmatory measurements of the longitudinal variance decay were done with a single hot wire.

The thermal field was scanned in the transverse direction by means of a precision traversing mechanism and stepping motor with minimum stepping increments of 5×10^{-5} in. (1.27×10^{-6} m).

3. The results

3.1. *The velocity field*

The decay of $\overline{u^2}$ and $\overline{v^2}$, the longitudinal and transverse mean-square velocity fluctuations, is shown in figure 2. The normalized variance decay laws deduced from this data are

$$\frac{\overline{u^2}}{U^2} = 0.121\left(\frac{x}{M}\right)^{-1.4}, \quad \frac{\overline{v^2}}{U^2} = 0.076\left(\frac{x}{M}\right)^{-1.32}, \tag{3),(4}$$

where the mean velocity $U = 7$ m/s. Various parameters of the velocity field are listed in table 1. Figure 3 shows u- and v-spectra at $x/M = 52$ and 103. From such spectra, 3-dimensional spectra were derived under the assumption of isotropy (Tennekes & Lumley 1972, chap. 8). The peaks of these spectra (not shown here) were at approximately $k = 1.3l^{-1}$ (m^{-1}), where l is the turbulence integral scale deduced from the velocity decay law (table 1). The peaks of these spectra are also listed in table 1 for various downstream locations.

3.2. *Single line source*

The results for the single line source were obtained primarily to provide background for the multiple line source interference study to follow. However, a number of new results for a single line source have been obtained in this study and hence the results

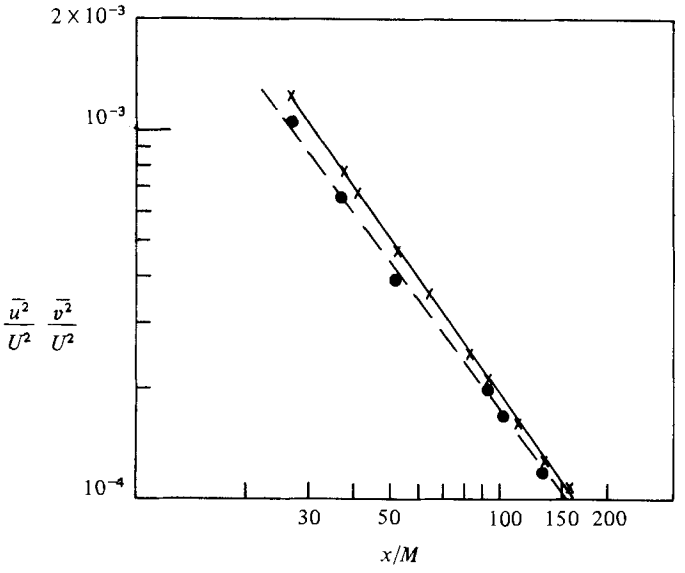

FIGURE 2. The decay of the longitudinal velocity variance $\overline{u^2}$ and the cross-stream variance $\overline{v^2}$: ×, $\overline{u^2}/U^2$; ●, $\overline{v^2}/U^2$. See also table 1.

	x/M			
	20	52	60	100
r.m.s. u (m/s)	0.299	0.153	0.139	0.097
r.m.s. v (m/s)	0.267	0.142	0.129	0.092
$\epsilon = -\frac{3}{2}(\mathrm{d}\overline{u^2}/\mathrm{d}t)$ (m²/s³)	2.63	0.265	0.188	5.53×10^{-2}
$l = (\overline{u^2})^{\frac{3}{2}}/\epsilon$ (m)	1.02×10^{-2}	1.35×10^{-2}	1.43×10^{-2}	1.65×10^{-2}
Peak of 3-dimensional velocity spectrum (m⁻¹)		98.5	87.4 ($x/M = 63$)	81.8 ($x/M = 103$)
$\lambda_g = (15\nu\overline{u^2}/\epsilon)^{\frac{1}{2}}$ (m)	2.86×10^{-3}	4.60×10^{-3}	4.97×10^{-3}	6.39×10^{-3}
$\eta = (\nu^3/\epsilon)^{\frac{1}{4}}$ (m)	1.99×10^{-4}	3.53×10^{-4}	3.84×10^{-4}	5.22×10^{-4}
η/l	1.95×10^{-2}	2.61×10^{-2}	2.69×10^{-2}	3.16×10^{-2}
$Re_l = ul/\nu$	191	129	124	100
$Re_\lambda = u\lambda_g/\nu$	53	44	43	39
$\tau_u = 3\overline{u^2}/\epsilon$ (s)	0.102	0.265	0.308	0.510

TABLE 1. Some characteristics of the velocity field. Re_M ($\equiv UM/\nu$) was 1.09×10^4 for all experiments; $U = 7$ m/s, $\nu = 1.6 \times 10^{-5}$ m²/s and $M = 0.025$ m.

are documented in considerable detail. During the course of this work the results of an experiment by Stapountzis *et al.* (1984) appeared. These measurements, which are more detailed than those of the previous measurements of a thermal line source by Uberoi & Corrsin (1953) and Townsend (1954), will be compared with the present results.

The development of the mean thermal wake in isotropic turbulence is generally divided into three stages: molecular diffusive, turbulent convective and finally turbulent diffusive (e.g. Stapountzis *et al.* 1984; Anand & Pope 1983). For the molecular-diffusive range ($t \ll \kappa/\overline{v^2}$, where κ is the thermal diffusivity) the spreading of the mean profile (based on its standard deviation σ_m or half-width) increases as

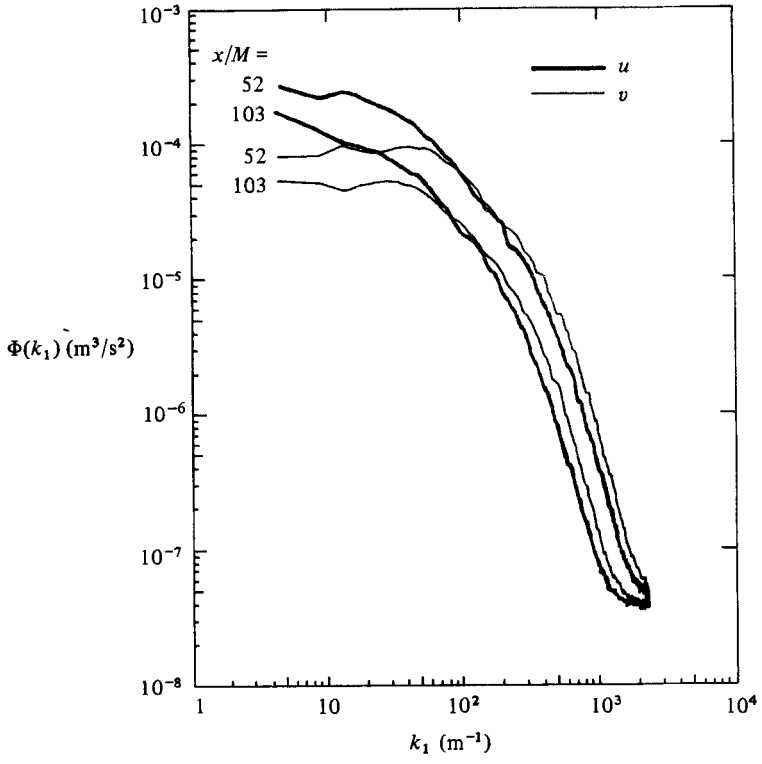

FIGURE 3. One-dimensional spectra of u and v at $x/M = 52$ and 103.

$t^{\frac{1}{2}}$: $\sigma_m = (2\kappa t)^{\frac{1}{2}}$. For the turbulent-convective range ($\kappa/\overline{v^2} \ll t \ll t_L$ where t_L is the Lagrangian timescale) the spreading rate is linear: $\sigma_m = (\overline{v^2})^{\frac{1}{2}} t$. Finally, for the turbulent-diffusive range ($t \gg t_L$) $d\sigma_m^2/dt \propto K_T$ (where K_T is the turbulent diffusivity), i.e. $\sigma_m \propto t^{\frac{1}{2}(2-n)}$ for grid turbulence. Here n is the decay exponent of $\overline{v^2}$. For $n = 1.32$ ((4) above) $\sigma_m \propto t^{0.34}$. Recently Anand & Pope (1983) have derived a quantitative relation, based on the probability-density-function method of Pope (1981) for all three stages of the evolution of σ_m. Their prediction will be compared with the present results.

Figure 4 shows the evolution of the mean centreline temperature, as well as the half-width of the mean profile, for a single wire placed at $x_0/M = 52$. The mean profiles (not shown) were Gaussian; their half-width is defined as half the width of the profile when its level is 50% of the maximum (centreline) value. The standard deviation for a Gaussian profile is 0.849 times the half-width. The ordinate y'/M refers to the lateral distance from the line source (figure 1). In order not to affect the velocity field close to the source, the fine (0.025 mm) wire was used for measurements up to and including $x'/M = 8.1$. In order to produce a larger temperature signal further downstream, the thicker wire (0.127 mm) was used for $x'/M \geqslant 8.1$. The power in the fine wire was 4.4 W/m, that in the thicker wire was 45 W/m. The curves match well. Note that the product of the half-width and the peak (centreline) temperature should be constant for a particular wire heating, as is observed. Also shown on figure 4(*a*) is the relation $(y'/M)_{\frac{1}{2}} = 1.18((\overline{v^2})^{\frac{1}{2}}/U)(x'/M)$, where $(y'/M)_{\frac{1}{2}}$ is the half-width of the mean profile. This is equivalent to $\sigma_m = ((\overline{v^2})^{\frac{1}{2}}/U)x'$ for a Gaussian profile and is the relation for the spreading of the mean-temperature profile in the convective range.

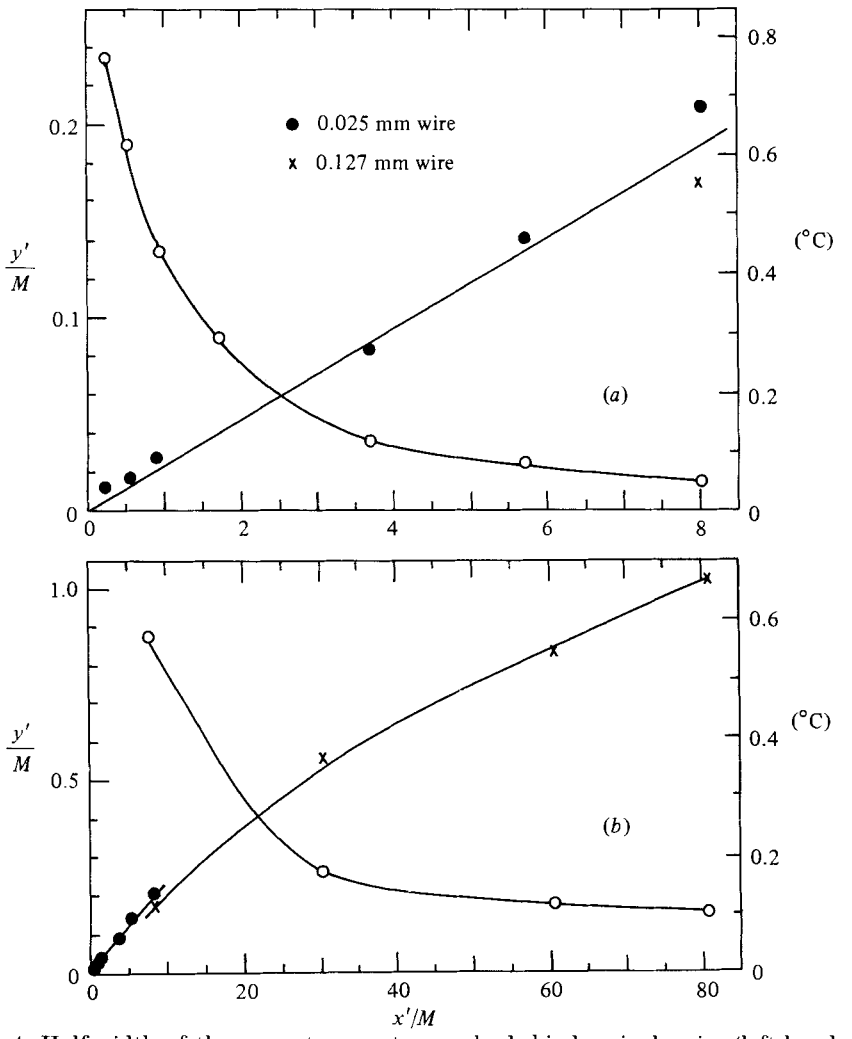

FIGURE 4. Half-width of the mean temperature wake behind a single wire (left-hand axis) and centreline (peak) temperature of the mean temperature profile (right-hand axis): (*a*) $x'/M \leqslant 8.1$, 0.025 mm heated wire; (*b*) $x'/M > 8$, 0.127 mm wire. Open circles are for peak temperature, filled circles and crosses are for the half-width. (*a*) also shows the line $(y'/M)_{\frac{1}{2}} = 1.18\,((\overline{v^2})^{\frac{1}{2}}/U)\,(x'/M)$.

It appears that the linear (convective) region extends to about $8M$ from the source. After that turbulent diffusion begins to become more important and the spreading rate is less rapid (figure 4(*b*) and figure 10 below).

Figure 5 shows the evolution of the half-width of the mean profiles for two other locations of the line source, $x_0/M = 20$ and $x_0/M = 60$. As would be expected, the closer to the grid the line source is placed (where the turbulence intensity is greater), the more rapid is the spreading rate of the mean profile. The form of the curves of figure 5 and the method of scaling them will be discussed below.

The downstream development of the r.m.s. θ-profiles, normalized by their centreline values, is shown in figure 6. As for the mean profiles, the 0.025 mm wire was used up to and including the distance $x'/M = 8.1$ from the source, thereafter the 0.127 mm wire was used. Notice that until approximately $x'/M = 1.8$ the r.m.s. profiles are double-peaked. This is presumably because near the source fluctuations are produced

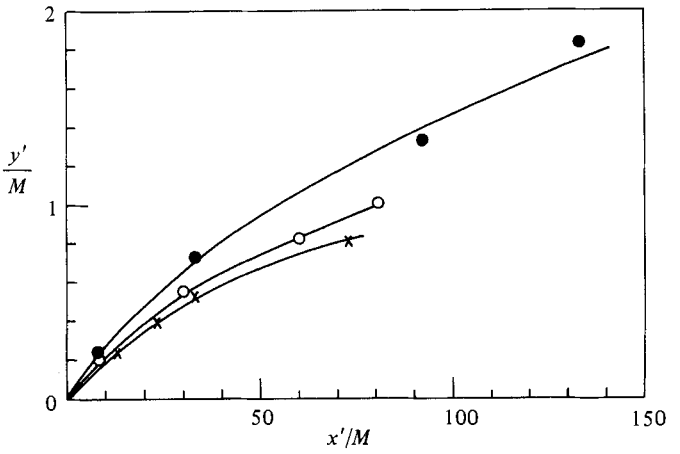

FIGURE 5. Half-width of the mean-temperature wake for the 0.127 mm wire placed at $x_0/M = 20$ (filled circles); $x_0/M = 52$ (open circles); $x_0/M = 60$ (crosses).

mainly by the bulk flapping of the wake, with little contribution from structure within it. Thus the largest gradients in temperature, and hence the highest values of r.m.s. θ will occur off the centreline, producing the double peak. The same effect was observed by Stapountzis *et al.* (1983) (see also Sawford 1984). After about $x'/M = 1.8$ the profiles become single-peaked. The ratio of the maximum value of r.m.s. θ to its centreline value, as a function of x'/M, is in agreement with the measurements of Stapountzis *et al.* (1984) (see figure 8 of their paper).

When the thermal line source was placed closer to the grid, the double peak in the r.m.s. θ-profile re-emerged far downstream. Figure 7 shows r.m.s. θ-profiles for the thermal source at $x_0/M = 20$. At $x'/M = 17$ the profile is single-peaked (as for the case where the source was placed at $x_0/M = 52$, figure 6). However, by $x'/M = 63$ a double peak has emerged and this is more pronounced by $x'/M = 133$. The re-emergence of the double peak does not appear to have been observed before by other workers owing to the limited downstream extent of their measurements. An explanation of this is wanting. Double peaks in the r.m.s. θ-profiles also re-emerged far downstream when the source was placed at $x_0/M = 5$.

The evolution of the ratio of the r.m.s. θ to the mean temperature T for the line source at $x_0/M = 52$ is shown in figure 8(*a*). The peak of r.m.s. θ/T is at about $x'/M = 10$, i.e. approximately at the end of the linear spreading region. Thereafter it appears to asymptote to a value of approximately 0.7. This final value is consistent with the observations of Uberoi & Corrsin (1953). Also plotted on the graph is the recent data of Stapountzis *et al.* Their values appear to be lower than ours for $x'/M > 2$. The peak does not appear in their work, but this may be due to insufficiency of their data points. The final value of r.m.s. θ/T for their data was 0.5 at $x'/M = 14.7$. Figure 8(*b*) shows the evolution of the half-width (50% of the centreline value) of the r.m.s. θ profiles of figure 6. Notice that the results for the fine wire match well with those of the thicker wire. The half-width of the r.m.s. θ-profiles are considerably larger than the half-width of the mean profiles; the ratio is approximately 1.5. Thus the half-width of $\overline{\theta^2}$ is approximately the same as that of T since the half-width of $\overline{\theta^2}$ is approximately $\sqrt{\frac{1}{2}}$ that of $(\overline{\theta^2})^{\frac{1}{2}}$. These results are in conformity with those of Stapountzis *et al.* (1984). We note also that, although the $\overline{\theta^2}$ profiles are non-Gaussian (figures 6 and 7), profiles of the total mean-squared

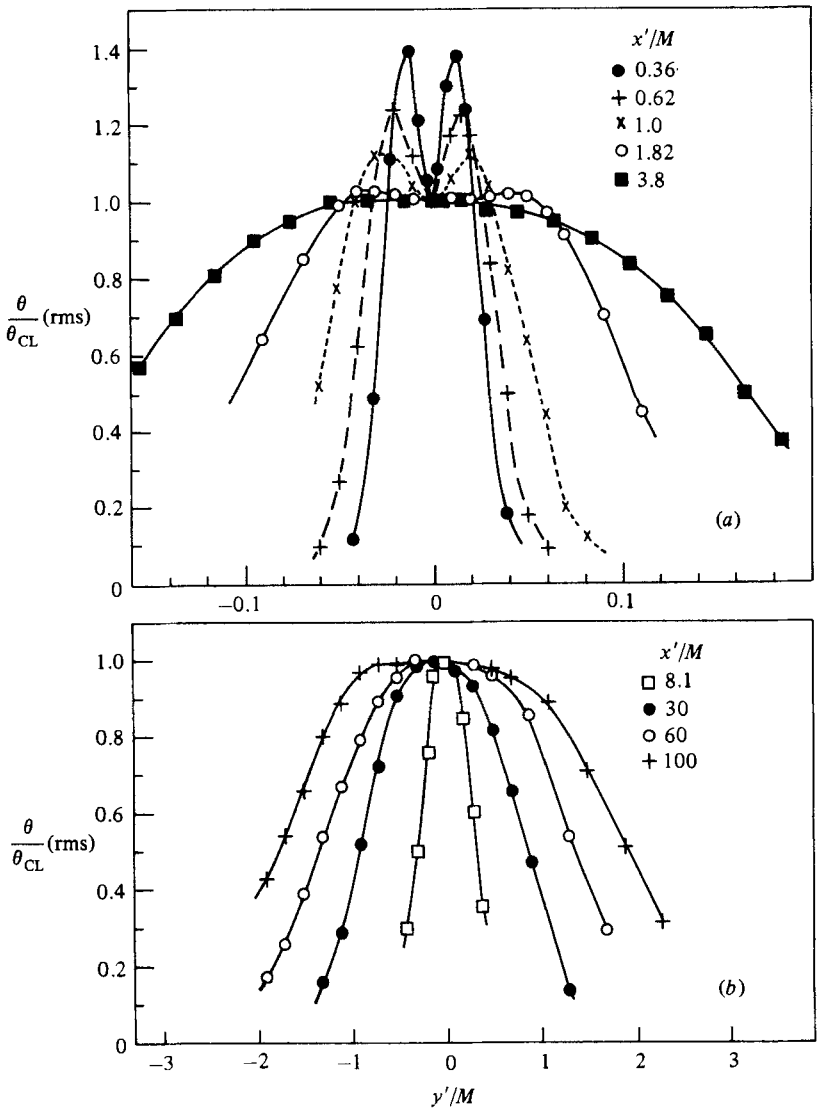

FIGURE 6. R.m.s. temperature profiles normalized by the centreline r.m.s. values. The wire was at $x_0/M = 52$. For measurements up to and including $x'/M = 8.1$, the 0.025 mm wire was used, thereafter the 0.127 mm wire was used.

temperature field $T^2 + \overline{\theta^2}$ (not shown here but easily constructed from the mean and r.m.s. profiles) were found to be Gaussian. This is also in accordance with the recent findings of Stapountzis *et al.*

Figure 9 shows the development of the r.m.s. half-width for the wire placed at $x_0/M = 5$, 20, 52 and 60. As for the mean profiles (figure 5), the closer the source is to the grid, the faster is the spreading rate.

The downstream development of the half-width of the mean and r.m.s. profiles of figures 5, 8(*b*) and 9 are summarized in figure 10. The half-widths of the profiles have been normalized by the integral scale at the location of the line source (table 1) and the distance downstream from the source has been normalized by the distance of the source from the grid. This scaling is suggested by Anand & Pope's (1983) modelling

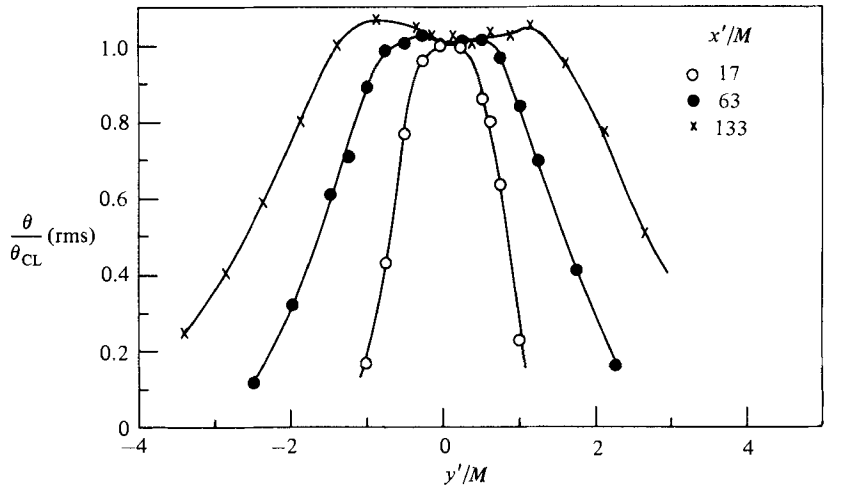

FIGURE 7. R.m.s. temperature profiles for the (0.127 mm) wire placed at $x_0/M = 20$.

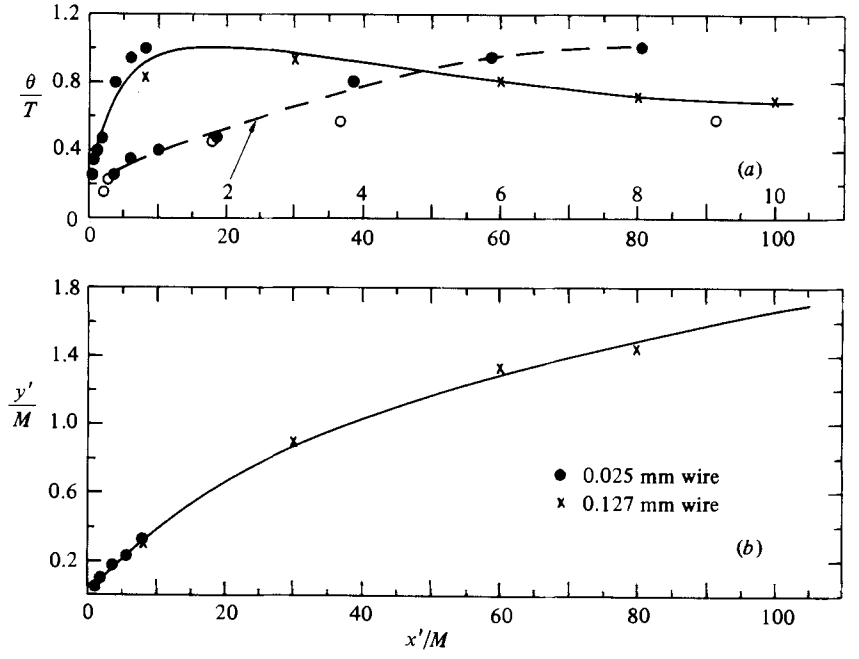

FIGURE 8. (*a*) R.m.s. θ/mean T, centreline values. For clarity the horizontal axis has also been amplified tenfold (dashed line) for the data points up to and including $x'/M = 8.1$. The data of Stapountzis *et al.* (1984) (open circles) are also shown on this amplified scale. (*b*) R.m.s. θ-profile half-width (based on centreline value). The wire was at $x_0/M = 52$ for both (*a*) and (*b*).

of a thermal wake and collapses the data taken at various x_0/M remarkably well. The Anand & Pope prediction for the mean-profile half-width, based on a conditional p.d.f. method (Pope 1981) is also shown on the graph. One adjustable constant (taken from the data) was used in their prediction. The fit to the data is excellent. Notice that even far downstream the diffusive range (where the slope of the curve should

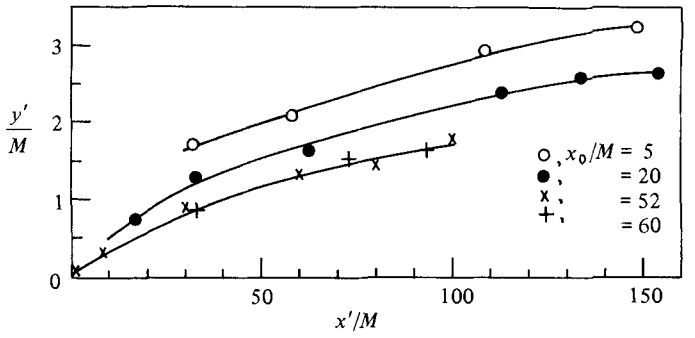

FIGURE 9. Half-width of the r.m.s. θ profiles for the wire at $x_0/M = 5$, 20, 52 and 60.

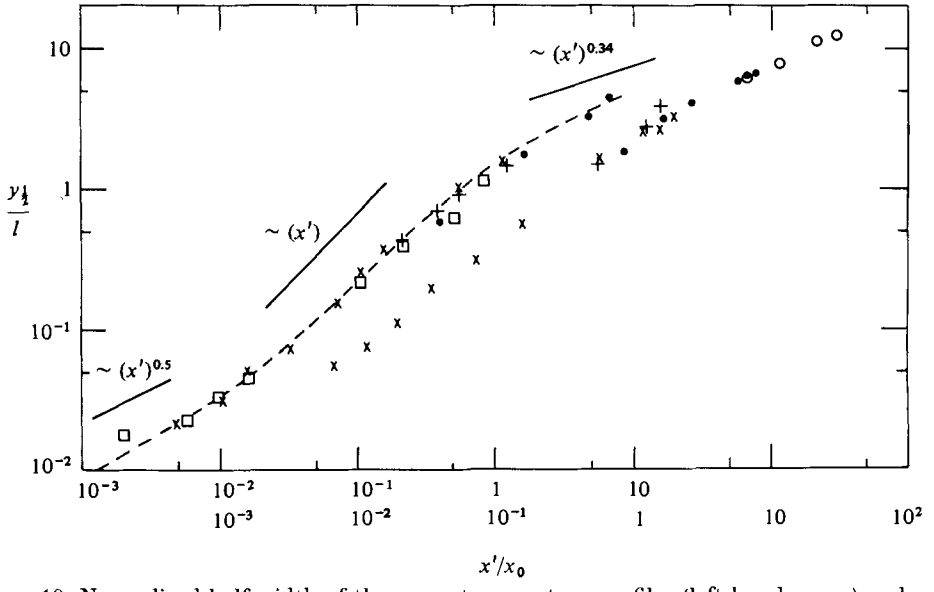

FIGURE 10. Normalized half-width of the mean-temperature profiles (left-hand curve) and r.m.s. temperature profiles (right-hand curve). The symbols (for the location of the source) for both the mean and r.m.s. profiles are the same as those used in figure 9. (The mean profiles were not measured for the wire placed at $x_0/M = 5$.) The open squares show the data (for the mean half-width) of Stapountzis *et al.* (1984). The dashed line is the prediction of Anand & Pope (1983).

be 0.34) is not reached. Also plotted on this graph are the recent data for the mean profiles of Stapountzis *et al.* (1984). Their values agree well with the present measurements. (The point closest to the wire of the Stapountzis *et al.* measurements (figure 10) suggests a slope less than 0.5, which is at variance with the scaling theory for the molecular-diffusive range. It is possible that resolution problems occurred in their measurements here.) The evolution of the r.m.s. θ half-width is also shown on figure 10. As for the mean half-width the collapse of the data is remarkably good for the line source placed at $x_0/M = 5$, 20, 52 and 60.

In order to check whether there was any dependence of wire (source) diameter on the evolution of the r.m.s. θ, a number of experiments were carried out with wires of different diameter, and with the tunnel operating at different speeds. Figure 11 shows r.m.s θ-profiles for the source at $x_0/M = 20$. For the wire Reynolds number

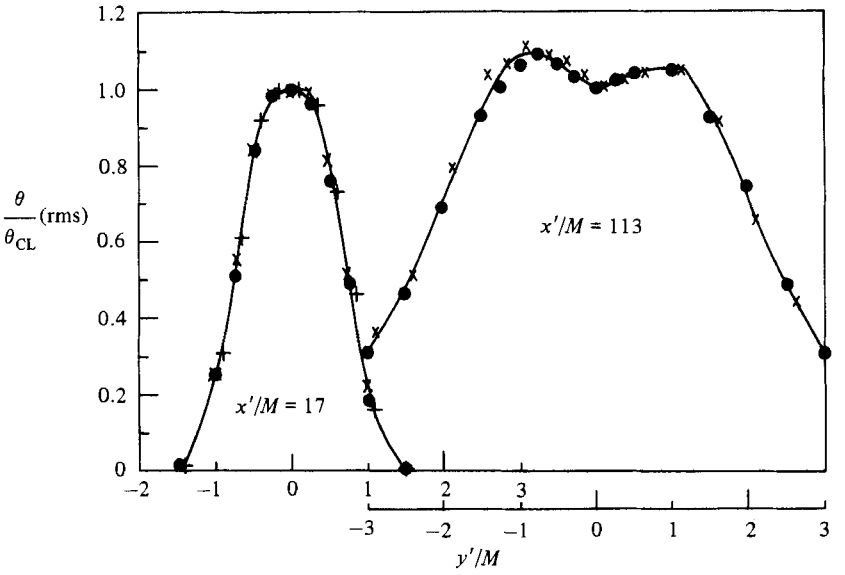

FIGURE 11. R.m.s. θ-profiles normalized by the centreline value for the wire placed at $x_0/M = 20$: ●, $Re = 39$ (wire diameter = 0.127 mm, $U = 4.8$ m/s); +, $Re = 175$ (wire diameter = 0.32 mm, $U = 8.5$ m/s); ×, $Re = 280$ (wire diameter = 0.51 mm, $U = 8.5$ m/s).

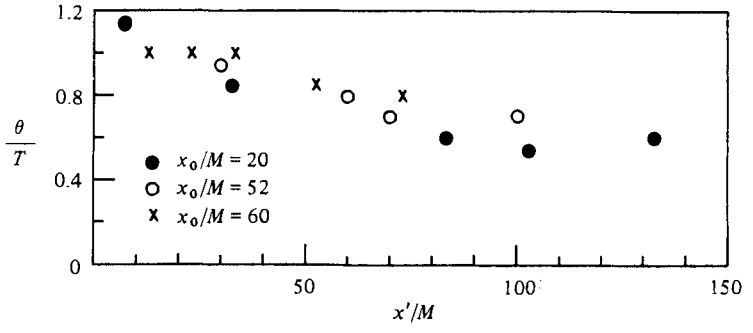

FIGURE 12. R.m.s. θ/mean T (centreline values) for the 0.127 mm wire placed at $x_0/M = 20$, 52 and 60.

varying from 39 to 280 there is virtually no difference in the profiles. This is consistent with the recent analysis of Sawford & Hunt (1983), who find that source size dependence occurs for $d \gg \eta$. Such a test was not carried out very close to the source because there vortex shedding would have affected the velocity field, thereby altering the nature of the experiment which was to study a passive scalar.

Finally, the ratio r.m.s. θ/T is shown (figure 12) for the source placed at $x_0/M = 20$ and $x_0/M = 60$, as well as at $x_0/M = 52$ (figure 8). For all positionings of the sources the value tends to asymptote to about 0.7.

3.3. *The interference of two line sources*

Extensive measurements of the interference of two line sources were carried out with pairs of wires placed at various downstream locations x_0/M and various spacings d (figure 1). First, measurements for the wires spaced at $x_0/M = 20$ will be described.

Figure 13 (lower curves) shows some examples of r.m.s. θ-profiles for three different wire spacings and for the probe located at three different locations from the sources.

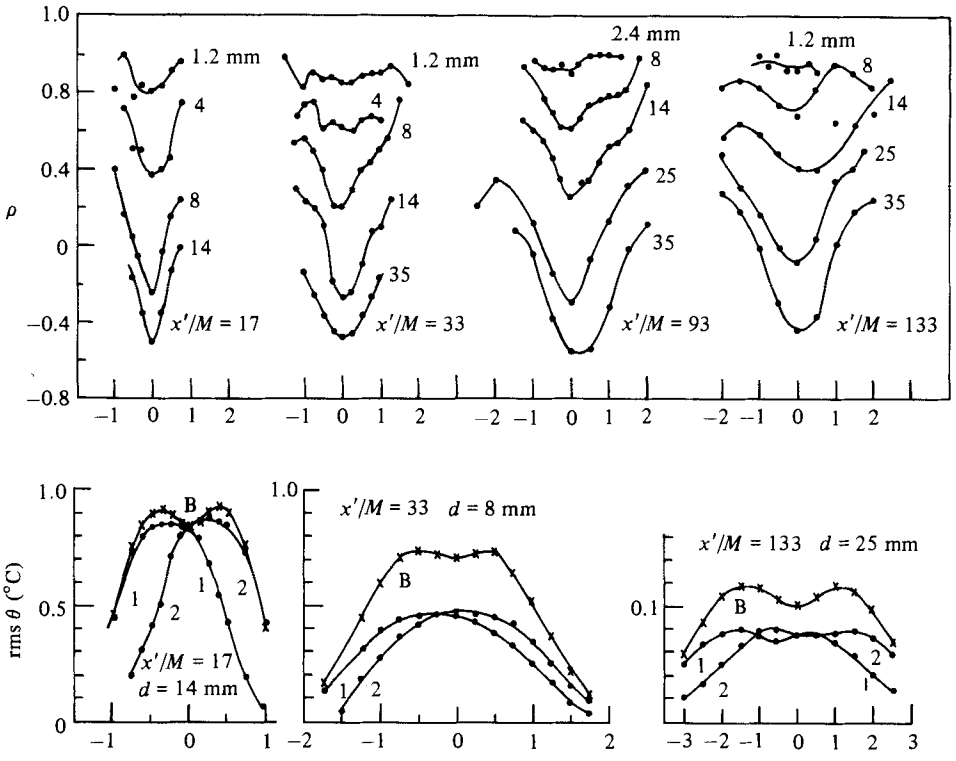

FIGURE 13. Bottom graphs show r.m.s. θ-profiles for a pair of wires operating separately (1 and 2) and together (B). Top graphs show ρ, inferred from graphs such as the bottom ones, for various d and x'/M. All horizontal axes are y/M. Wires are at $x_0/M = 20$.

The integral scale l for $x_0/M = 20$ is listed in table 1. Curves 1 and 2 (figure 13, lower graphs) are for each wire operating separately, and B is for both wires operating together. Note that along the centreline between the two wires there is a dip in curve B, since here the interference between the two wires is the strongest. Notice also, for $x'/M = 133$, the two r.m.s. profiles for each wire operating separately also has a dip, as discussed in the previous section. From such profiles as these, the upper curves of figure 13 were obtained by solving (1) for ρ, viz

$$\rho = \frac{\overline{\theta_B^2} - \overline{\theta_1^2} - \overline{\theta_2^2}}{2(\overline{\theta_1^2})^{\frac{1}{2}}(\overline{\theta_2^2})^{\frac{1}{2}}}. \tag{5}$$

These curves show the variation of ρ as the field is traversed in the y-direction for a particular value of x'/M. The curves have distinct minima at the points intermediate between the two wires ($y = 0$, figure 1), but these minima tend to become less pronounced for small d and large x'/M, as would be expected. The width of the curves also becomes greater for larger x'/M. From such families of curves figure 14 was produced. These correlation coefficients are for the probe location at $y = 0$ and include values of d and x'/M not shown on the upper curves of figures 13.

The evolution of ρ is clearly a function of d (or more generally d/l, see below). For very small d the cross-correlation coefficient rapidly increases from a value that appears to commence at -1, to a value close to $+1$. When the sensor is close to the wires, we would expect ρ to be negative. This follows if we write

$$\rho = (\overline{T_1 T_2} - T_1 T_2)/(\overline{\theta_1^2})(\overline{\theta_2^2})^{\frac{1}{2}},$$

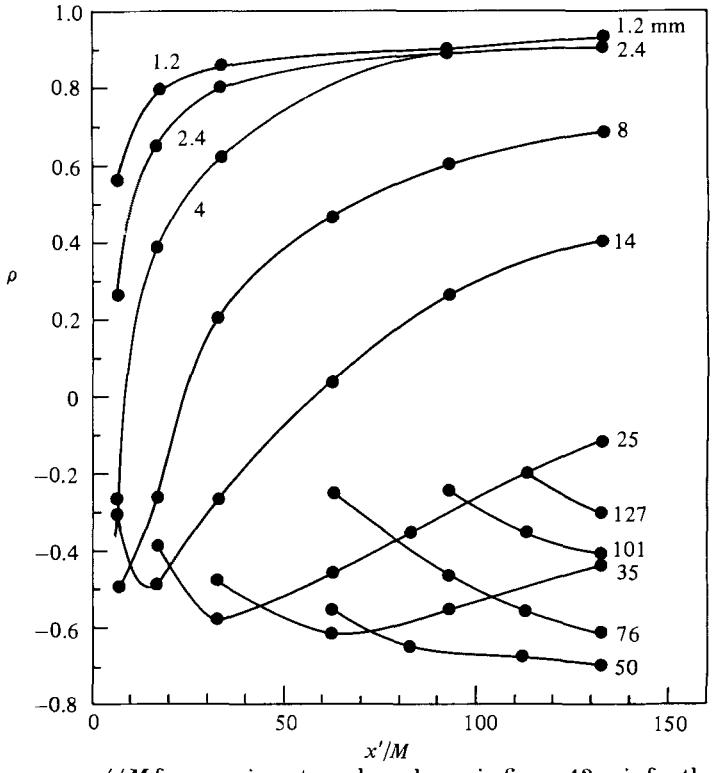

FIGURE 14. ρ versus x'/M for experiments such as shown in figure 13. ρ is for the midpoint between the wires ($y = 0$, figure 1). The numbers are the wire spacing d (mm). The wires are at $x_0/M = 20$.

where Υ is the total instantaneous temperature $T+\theta$. If the plumes never overlap instantaneously $\overline{\Upsilon_1 \Upsilon_2} = 0$ and $\rho < 0$. As the wakes begin to merge together (increasing x') ρ rises to a value of $+1$ (when the wakes are completely mixed). As d is increased (e.g. $d = 4$ mm) this merging process occurs at a slower rate. For large d (the effect is clear for $d > 8$ mm), ρ first decreases and then begins to increase. For these cases the sensor may initially sample one wake or the other (but not both). However, it will mainly be sampling ambient air and ρ will be close to zero. As the two wakes begin to broaden (i.e. as x'/M increases) less of the time will be spent sampling ambient air and the negative correlation will build up. However, mixing of the two wakes will also begin to occur and this has the effect of reversing the negative trend in ρ; the mixing will drive ρ in the positive direction as for the small-d case. Notice that for $d > 50$ mm only the initial decrease in ρ is observed. Also, for these larger d, no meaningful value of ρ could be determined for small x'/M since the wakes did not cross the centreline. Of course, even for very small d, ρ should also first decrease and then increase as x'/M increases. Figure 15 shows ρ as a function of x'/M for small values of x'/M with $d = 1$ mm. Here the 0.025 mm wires were used and they were placed at $x_0/M = 52$. For $x'/M < 1$ ρ does not indeed appear to be asymptoting to -1 but shows the beginnings of the reversal exhibited for larger d. The cross-correlation coefficient was not measured for $x'/M < 0.36$. The minimum value for ρ is around -0.9 for the close wire spacing of figure 15, whereas for the larger wire spacing it is closer to -0.7 (figure 14). This is because for small d the wakes are being flapped in synchronism (in the convective range), whereas for larger d (and thus larger d/l) the wakes are less synchronous (and thus there will always be pockets

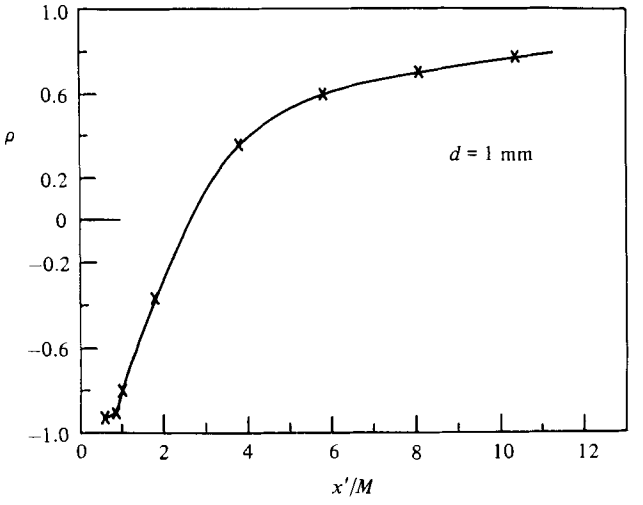

FIGURE 15. $\rho(y = 0)$ as a function of x'/M for the 0.025 mm wires spaced 1 mm apart at $x_0/M = 52$.

of ambient air between them) since they are affected by different parts of the velocity field.†

The effect of varying d but holding the probe at a particular downstream location is shown in figure 16(*a*), which is a replot of figure 14. Also shown in figure 16 is ρ as a function of d for the wire pairs placed at $x_0/M = 5$ and 60. As the wire separation is increased, ρ decreases from its initial value near unity; however, this trend reverses for large separation, for the reason described above. Note that, as x'/M decreases, the reversal occurs for smaller d as would be expected. None of the curves of figure 16 achieve a value of $\rho = 1$ for large x'/M as $d \to 0$. (This is also apparent from figure 14.) The reason for this is unclear. (We note that the reproducibility of the results was extremely good; on repeated experiments ρ varied only by about ± 0.03 for a particular x'/M and d.) The results of figure 16 also suggest that ρ tends to zero for large d. For this case the wire samples one wake or the other, but most of the time it is sampling ambient air.

For the fine wires used in this experiment the evolution of ρ is independent of wire diameter and is a function of u/U, l, d and x' only. For the experiments described here all of these parameters were varied. Figure 17 summarizes the results of these experiments. Most of the measurements were done for $x_0/M = 5$, 20 and 60, with less extensive measurements for $x_0/M = 42$ and 52. The two dimensionless variables chosen have been d/l and $(x'/d)(u/U)$. The latter variable may be thought of as the time to the probe x'/U non-dimensionalized by the lateral convective timescale d/u. Strictly d/v should have been used for this latter timescale, but the turbulence is close to isotropic and u is only a few percent different from v (table 1). Furthermore, sine the turbulence is decaying this convective timescale should be an integrated value

† If the instantaneous wakes could be represented by rectangular profiles, then a minimum value of $\rho = -1$ would occur when the probe senses one wake or the other but not both at the same time *nor* ambient air, i.e. when they are flapped over small angles in synchronism (the case of small d and close to the wires). In fact, close to the wires, the instantaneous profiles are Gaussian, and therefore even for synchronous flapping over a small angle with no ambient air between the wakes ρ will not equal -1, because of the nonlinear profile of the wakes: an increase in temperature from one wake will not correspond to precisely an equivalent decrease from the other. However the departure from perfect anticorrelation appears to be small (figure 15).

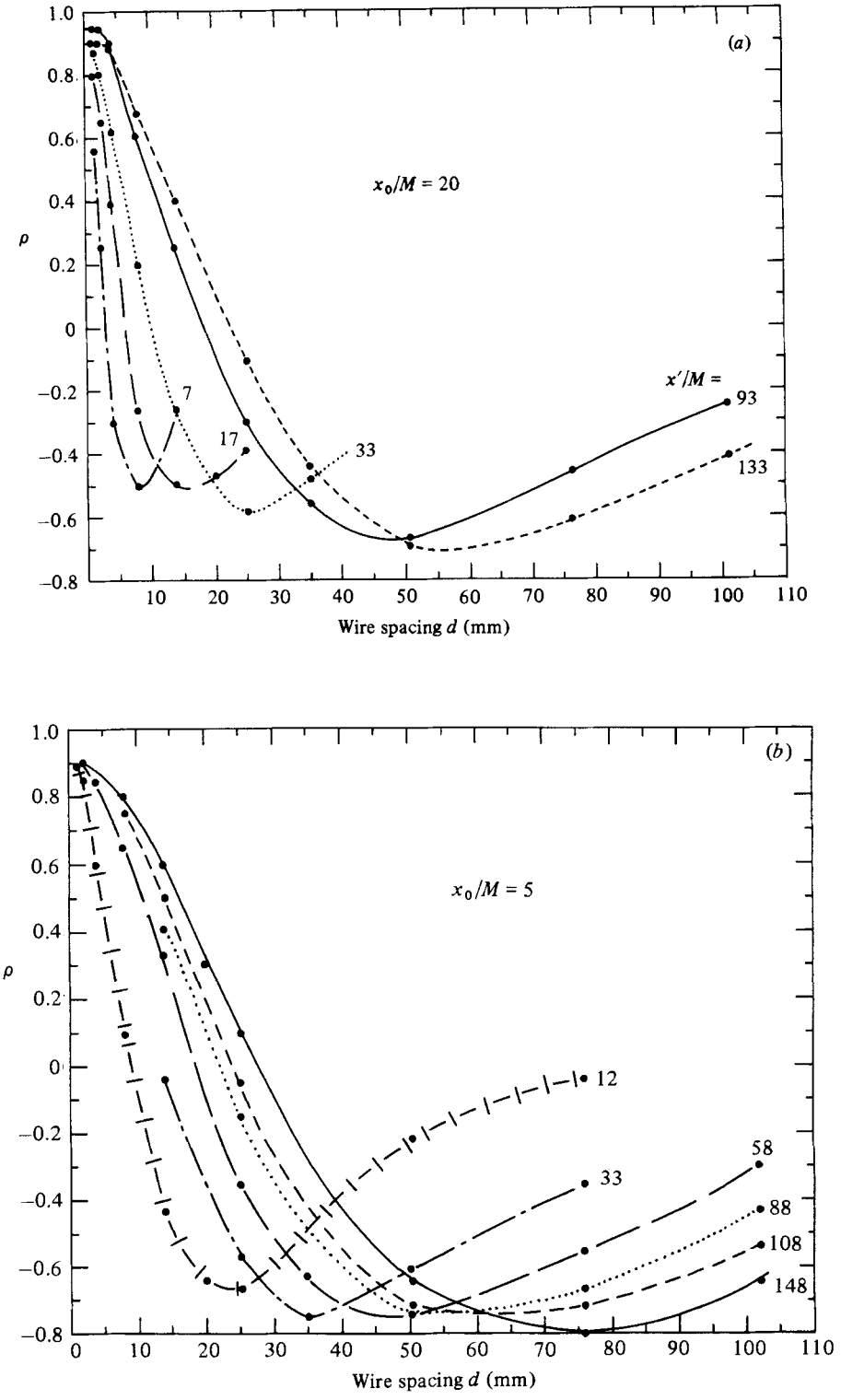

FIGURE 16 (a,b). For caption see facing page.

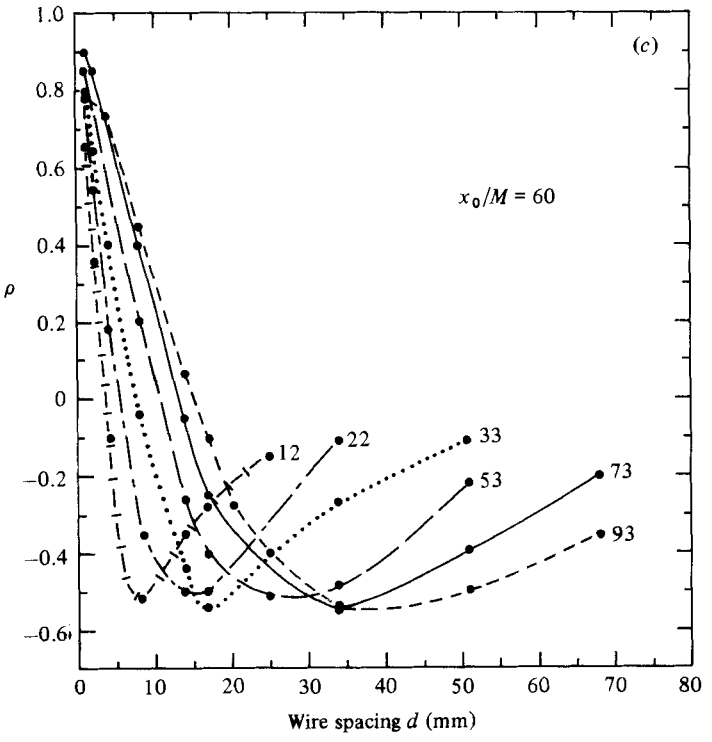

FIGURE 16. (*a*) Replot of figure 14. ρ versus d for various values of x'/M (labelled on the graph). (*b*) and (*c*) same as (*a*) but for the wires at $x_0/M = 5$ (*b*) and $x_0/M = 60$ (*c*).

of u from the source to the probe location. Nevertheless, using this simple scaling the data of figure 17 collapse remarkably well, even for the source location at $x_0/M = 5$ where the turbulence is far from homogeneous. The trend of the curves is similar to those of figure 14.

It is unfortunate that the nature of the evolution of ρ prevents us from determining its large-t asymptotic value (as a function of d/l) despite the relatively long downstream extent of our measurements. This is particularly so for large d/l (figure 17*b*). Even for small d/l, while the curves of figure 17(*a*) suggests ρ may be asymptoting to $+1$ far downstream, the alternative plots of figure 16 indicate that ρ does not appear to approach this limit, as is noted in the previous paragraph.

Figure 18 shows $1+\rho$ as a function of d/l for a number of values of $(x'/d)(u/U)$. Various regimes are clearly apparent from this plot. Consider, first, moderate normalized times from the source ($(x'/d)(u/U) = 2$ and 4, figure 18). There are three distinct regions. For d/l less than approximately 0.7, $1+\rho$ decreases relatively slowly as a function of d/l. The slope also decreases as $(x'/d)(u/U)$ is increased from 2 to 10. Unfortunately there is no inertial subrange for these relatively low-Reynolds-number experiments (figure 3), and the condition $\eta \ll d \ll l$ is not met. Thus the inertial-subrange model of Durbin (1980), which is applicable to this type of problem, cannot be tested in its present form from these measurements. The second region, $1 < d/l < \sim 7$ (figure 18, $(x'/d)(u/U) = 2, 4$ and 5) shows a much more rapid decrease of $1+\rho$. Possibly this is a diffusive range, but it will require detailed analysis to predict the form of $1+\rho$ for this region. Thirdly, the trend in the curves reverses for large d/l. This is the region in which the wakes from the individual curves have not yet

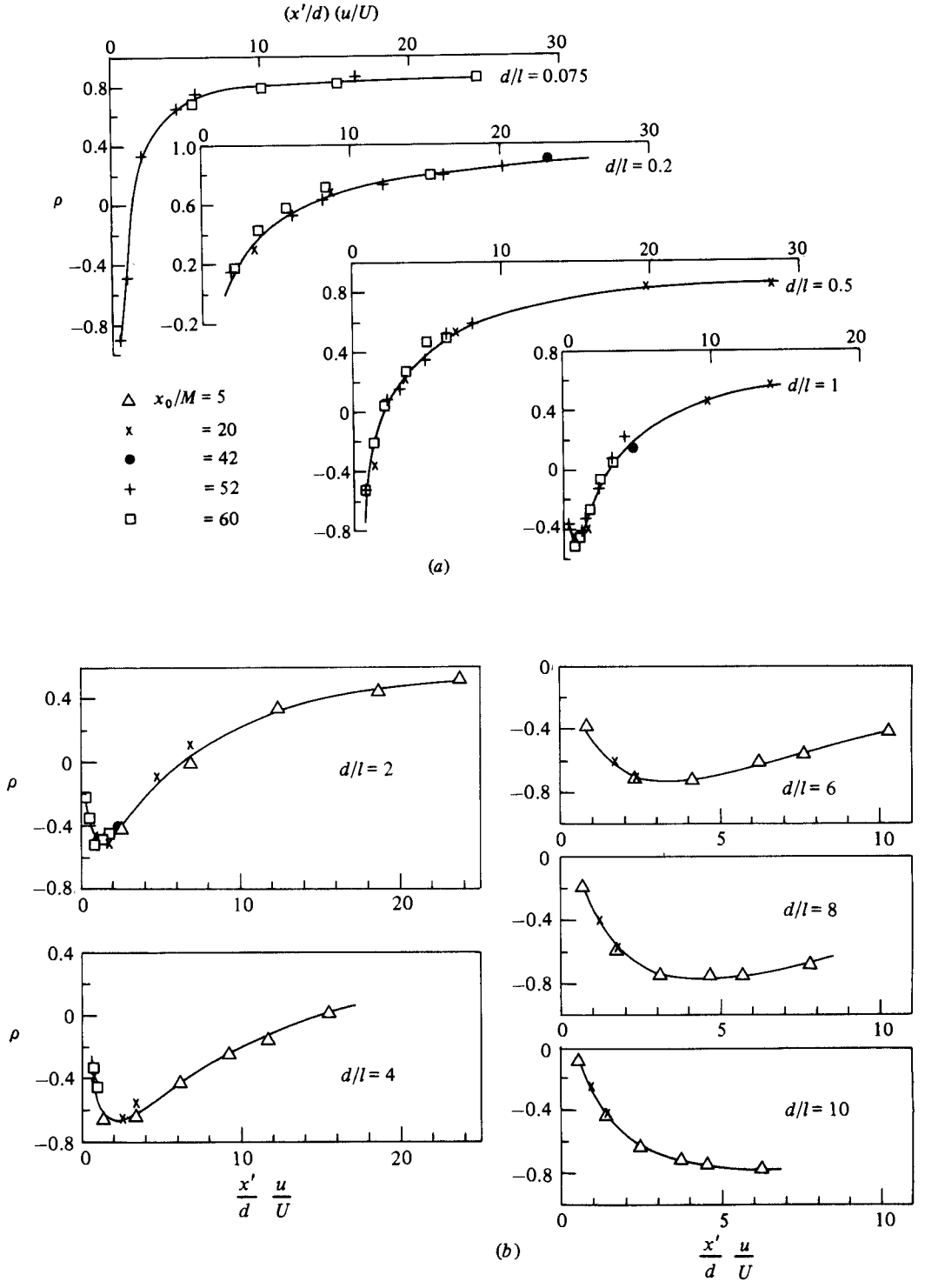

FIGURE 17. ρ versus normalized (convective) time $(x'/d)\,(u/U)$ for pairs of wires located at $x_0/M = 5$, 20, 42, 52 and 60. l is calculated at the x_0/M location of the wires. (*a*) d/l varying from 0.075 to 1; (*b*) d/l varying from 2 to 10.

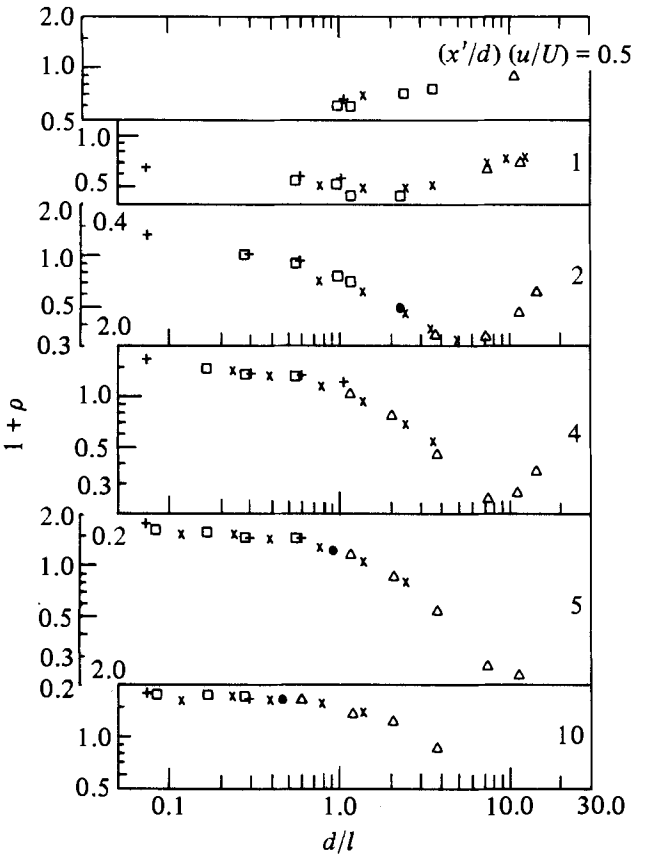

FIGURE 18. $1+\rho$ versus d/l for various normalized (convective) times. The symbols are the same as figure 17.

merged and mixed. For small $(x'/d)\,(u/U)$ (two upper curves of figure 18) this regime begins to occur much earlier, as would be expected, because of the short (non-dimensionalized) time from the probe.

A linear–log plot of ρ versus d/l also reveals the same three regions as figure 18.

3.4. *The interference of multiple line sources*

As stated in §1, one of the objectives of this experiment was to gain a greater understanding of the dissipation of scalar variance in homogeneous turbulence. In a previous experiment Warhaft & Lumley (1978) injected the scalar field into decaying grid turbulence by means of a mandoline, a set of equally spaced parallel line sources located downstream of the grid. Previous to that experiment heated grids had been used to study scalar variance decay, with ambiguous results (Warhaft & Lumley 1978). By changing the spacing of the mandoline wires, or by changing the distance from the grid that the mandoline was situated, Warhaft & Lumley showed that the scale of the scalar field was altered relative to that of the velocity field. As this lengthscale ratio was altered, so, it was found, was the rate of scalar-variance decay, and hence the rate of dissipation of scalar variance. Thus the scalar dissipation rate was directly related to the relative scales of the scalar and velocity field. Implicit in that study was the notion that the scalar field became homogeneous relatively quickly in the decaying, homogeneous turbulence. We will show here that the scalar variance

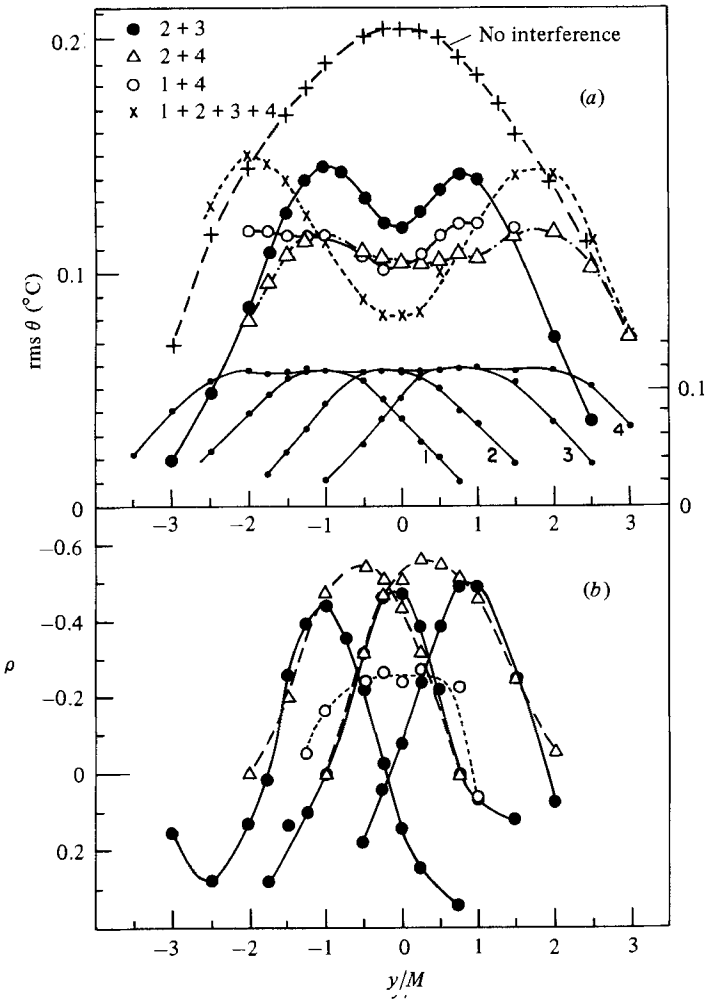

FIGURE 19. Top graph shows r.m.s. θ-profiles measured at $x'/M = 63$ for various combinations of four heated wires (labelled on the graph) spaced $1M$ apart and located at $x_0/M = 20$. The transverse locations of the wires are $y/M = -1.5$, -0.5, $+0.5$ and $+1.5$. Left-hand axis is for the various combinations (wire 2+wire 3, etc.), right-hand axis is for the r.m.s. profiles of each wire (1, 2, 3 and 4) operating separately. Bottom graph shows ρ inferred from the top graph. Dots, pairs of wires $1M$ apart (wires 1 and 2, 2 and 3, 3 and 4); triangles, pairs $2M$ apart (wires 1 and 3, 2 and 4) open circles, the pair of wires 1 and 4 ($3M$ apart).

produced by the mandoline may be thought of in an entirely different way: its magnitude and rate of decay can be viewed as due to the interference of multiple line sources.

Figure 19(*a*) shows the individual r.m.s. θ-profiles for four line sources located at $x_0/M = 20$, with wire spacing $1M$ apart. Also shown in the figure is the effect of operating the line sources in various combinations, as well as the value of r.m.s. θ if no interference were present ($\rho = 0$, equation 1). Note that if extra wires were added to the set (placed $1M$ apart) for this downstream location ($x'/M = 63$) the centreline ($y/M = 0$) value of the total r.m.s. θ would hardly be affected because the spread of the r.m.s. θ-profiles would be insufficient to reach $y = 0$ (consider the addition of wire 5 placed at $y/M = 2.5$ for example). Thus a mandoline, for this x'/M, can be

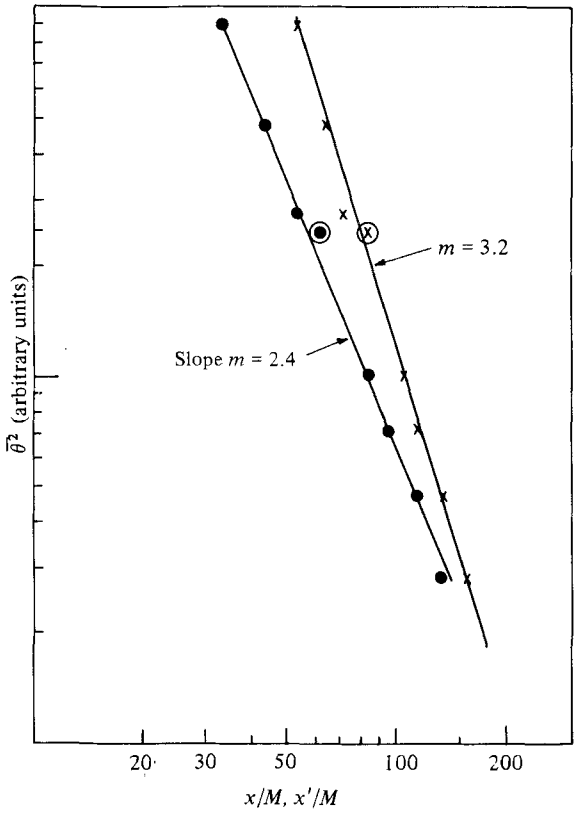

FIGURE 20. $\overline{\theta^2}$ decay for a mandoline (wires $1M$ spacing) at $x_0/M = 20$. Crosses, $\overline{\theta^2}$ versus x/M; dots, $\overline{\theta^2}$ versus x'/M. The circled cross and dot shows the value of $\overline{\theta^2}$ for only four wires of the mandoline operating (figure 19).

considered as consisting of four interfering wires only. (Closer to the source fewer wires will be needed, further away, more). The effect of the interference of the four line sources at this location is to reduce the total r.m.s. produced by the four individual line sources by greater than a factor of two (figure 19*a*), and hence the variance by greater than a factor of four. Figure 19(*b*) shows the cross-correlation profiles for the data of figure 19(*a*). The peak values of these curves are, of course, the same as the values of ρ at $x'/M = 63$ for wire spacings 25, 30 and 76 mm ($1M$, $2M$ and $3M$) shown on figure 14. It is clear from figure 19 that knowledge of $\rho(x', y)$ as well as the evolution of the r.m.s. of a single wire is sufficient to predict the evolution of the total scalar variance since (2) can be solved for this quantity. Note that curves such as figures 14 and 17 only contain information on $\rho(x')$ along the centreline between the two wires. In order to solve (2), off-centreline values of ρ must be known, such as those shown in figures 13 and 19(*b*). This is apparent from studying the values of ρ at $y/M = 0$, in figure 19(*b*). However, the curves of figures 14 and 17 clearly show the dependence of the centreline ρ on wire spacing and thus the reason for different decay rates of $\overline{\theta_T^2}$ when the mandoline wire spacing, or the distance from the grid of the mandoline, is changed.

Figure 20 shows the decay of $\overline{\theta^2}$ for a full mandoline (all wires operating). Also shown is the value of $\overline{\theta^2}$ for $x'/M = 63$ (figure 19*a*). It is clear that the interference of four fields at this location produces the same variance as a full mandoline (i.e. a set of wires

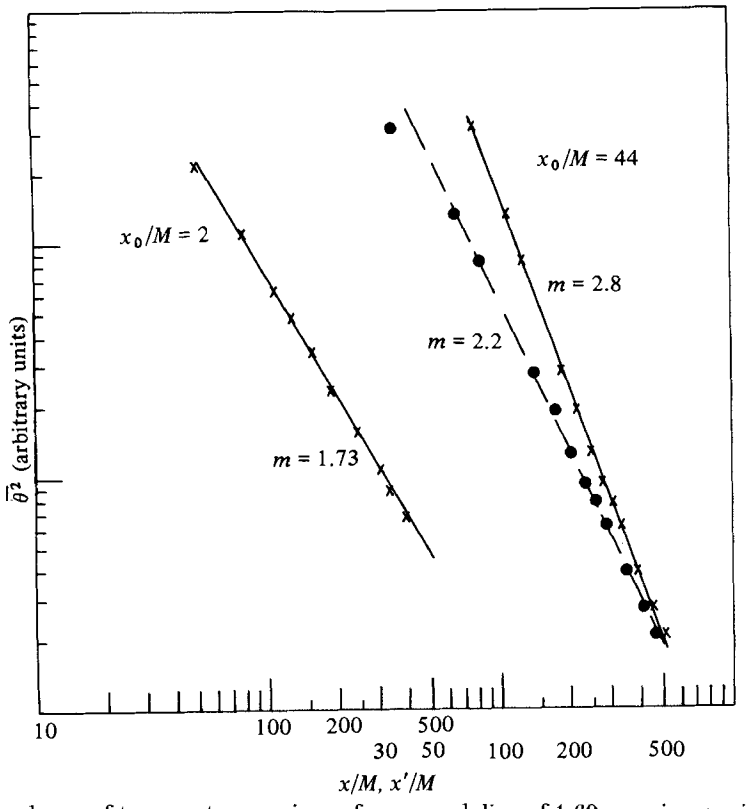

FIGURE 21. The decay of temperature variance for a mandoline of 1.69 cm wire spacing placed at $x_0/M = 2$ (left-hand graph) and $x_0/M = 44$ (right-hand graph) from the grid. $M = 0.84$ cm. Crosses, $\overline{\theta^2}$ versus x/M; dots, $\overline{\theta^2}$ versus x'/M.

$1M$ apart for the full cross-section extent of the tunnel). Other examples such as shown in figure 19 were examined for the wires at different x_0/M, and these, giving different interference patterns, produced different values of the variance and thus different decay rates of the total variance.

An interesting feature of the curves shown in figures 14 and 16–18 is the relatively long period it takes for the wakes of two wires to mix for any wire spacing that is an appreciable fraction of the integral scale. In our previous mandoline studies, the streamwise extent of the tunnel was less than $200M$. Although this is greater than one turbulence turnover time, it may be conjectured that, if the tunnel were longer, a trend to an equilibrium decay rate would be observed. Figure 21 shows measurements of $\overline{\theta^2}$ done with a grid of $M = 0.847$ cm, one-third the value used by Warhaft & Lumley (1978). Thus the tunnel is effectively extended by a factor of three to nearly $500M$. A mandoline (of $\frac{2}{3}M$ wire spacing) was placed at $x_0/M = 2$ and at $x_0/M = 44$. Notice that there is no tendency for the slope of the curve to equilibrate to a constant value. When considered from the viewpoint of interfering line sources this result is not surprising in view of the long time it takes for mixing to occur (figure 17). We also note that the strong dependence of ρ on wire spacing (figure 17) explains the difference in the results between Warhaft & Lumley (1978) and Sreenivasan *et al.* (1980). For the latter measurements the wire spacing was such that $d/l \lesssim 1$, while for the former $d/l > 1$.

4. Discussion

The results pose interesting questions concerning our present notion of scalar dissipation. For decaying isotropic turbulence, the rate of decay of the turbulence energy $\overline{q^2} = \frac{3}{2}\overline{u^2}$ is described by the equation

$$\frac{\mathrm{d}\overline{q^2}}{\mathrm{d}t} = -\nu \overline{\frac{\partial u_i}{\partial x_j}\frac{\partial u_i}{\partial x_j}} \equiv -\epsilon, \tag{6}$$

while for an isotropic scalar field the variance decay law is

$$\frac{1}{2}\frac{\mathrm{d}\overline{\theta^2}}{\mathrm{d}t} = -\kappa \overline{\frac{\partial \theta}{\partial x_j}\frac{\partial \theta}{\partial x_j}} \equiv -\epsilon_\theta. \tag{7}$$

The prevailing interpretation of (6) is in terms of the Kolmogorov model; the destruction of turbulence energy is due to the cascade of the energy from large to small scales, where it is finally converted into internal energy by the viscosity of the fluid. By analogy (equation 7), we think of the destruction of scalar variance in a similar way (Tennekes & Lumley 1972): scalar fluctuations introduced at large scales undergo a cascade to smaller scales where they are finally smeared by molecular action.

The mandoline experiments of Warhaft & Lumley (1978) and the related experiments of Sreenivasan *et al.* (1980) have previously been interpreted in this light. For a specified wire spacing the thermal field was inserted into the turbulence at a particular scale or wavenumber and a cascade then ensued to higher wavenumbers (or smaller scales) until the thermal diffusivity smeared the fluctuations. As the wire spacing was varied so was the input scale (as is shown by temperature spectra (Warhaft & Lumley, 1978)). The higher the input wavenumber (and hence the closer to the dissipation scale) the scalar was injected, the faster was the variance decay rate. Essential to this picture was the assumption that the scalar field was homogeneous. This assumption was believed to be sound from transverse profiles of the mean and r.m.s. thermal field (which were flat) and from the nature of the temperature spectra. By invoking the assumption of a homogeneous scalar field Antonopoulos-Domis (1981) and Herring *et al.* (1982) were able to reproduce the mandoline results using numerical methods.

The present results show, however, that the mandoline may be considered in a different way, i.e. the interference of inhomogeneous line sources. Viewed in this way, the simple cascade model is inadequate to describe the results since production and advection must also be accounted for in order to predict the evolution of the total thermal variance. Alternatively, the present results suggest that the mandoline may be considered as producing destructive (and dissipationless) interference between the line sources. This interference accounts for the variation in scalar variance destruction as the wire spacing is changed. Thus the scalar-variance dissipation is partly due to interference and partly due to molecular smearing.

That these interpretations (homogeneous thermal field *vs.* inhomogeneous interfering line sources) are consistent with each other, is shown in a previous experiment. In Sirivat & Warhaft (1983) a linear temperature gradient was established using differentially heated mandoline wires. This experiment can be interpreted as the interference of a number of differentially heated line sources, and the results could be predicted using information such as that shown in figure 17. In that study a completely different method of establishing a linear temperature gradient was also used: the gradient was formed in the laminar flow before the grid in the plenum

chamber of the tunnel. For this method, the temperature variance was produced solely by the interaction of the linear gradient with the grid turbulence. This is close to the notion of injecting a homogeneous thermal field into the grid turbulence. Yet the results of these two experiments were essentially the same: equilibrium values of the thermal length- and timescales obtained using the differentially heated mandoline wires were very close to those obtained using the linear temperature profile inserted upstream from the grid. This result suggests that although a mandoline may (fundamentally) be considered to be composed of interfering inhomogeneous line sources it is also compatible with the notion of inserting a homogeneous scalar field at specified scale. Possibly a two-particle dispersion theory based on the relative motion of marked molecules such as that recently developed by Sawford & Hunt (1984) or the conditional p.d.f. method of Pope (1981, 1983) will provide further insight into the basic problem of what occurs when a scalar is injected into a turbulent field.

5. Conclusions

The experimental results described here have been concerned with the evolution of the mean and variance of the thermal field downstream of single and multiple line sources.

The single-line-source measurements show that the variance or r.m.s. θ-profiles exhibit a double peak very close to the source and also very far downstream where the diffusive region is beginning to prevail. In between these regions the r.m.s. profile is single-peaked. The mean profiles for these experiments were Gaussian at all positions. The data for the spreading rate of the mean and r.m.s. profiles collapse well using values of the turbulence integral scale measured at the source (whose position was varied from $x_0/M = 5$ to $x_0/M = 60$). The trend of the spreading-rate results are in good agreement with those of Stapountzis *et al.* (1984) (which were only done for one downstream location of the source). No dependence of the evolution of the thermal field on wire Reynolds number was observed for $39 < Re < 280$ for moderate-to-large distances ($x'/M > 8$) from the source. The dependence on Re close to the source was not studied since vortex shedding would have changed the objective of the present study which was to study a passive scalar. Thus for measurements very close to the source, a very fine wire ($Re = 11$) was used. These results matched well (at $x'/M = 8$) with the higher-Re measurements.

The experiments concerning two and multiple line sources show that the mixing of thermal wakes downstream from the sources is a strong function of d/l and that for d/l of order unity complete mixing of the wakes is not achieved even far downstream. It is concluded that the mandoline can be considered as a set of interfering thermal fields produced by multiple line sources. This interpretation suggests that scalar variance may be considered as being destroyed, in part, by (dissipationless) destructive interference; similar to the interference that occurs in wave motion. The results should enable the recent pair-dispersion theories of Durbin (1980), Sawford (1983) and Sawford & Hunt (1984) to be tested in detail.

Finally we note that other scalar fields such as a thermal mixing layer or a linear temperature gradient may be considered in terms of multiple-line-source interference. Futhermore the method of approach used here could be used to investigate scalar mixing in flows other than grid turbulence, such as wakes, jets, etc. The inference method can be used in any flow that is statistically stationary.

I thank Mr D. Boxley for his careful assistance with the extensive measurements. Messrs E. P. Jordan, N. R. Panchapakesan and Bai-kun Ma were also of valuable

assistance in the experimental work. I also thank Professor S. B. Pope for insightful discussions and suggestions and Professor J. L. Lumley, Dr B. L. Sawford, Dr A. Sirvat and a referee for helpful comments on the first draft of this work. This work was funded by grants from the Engineering section and the Atmospheric Science section of the U.S. National Science Foundation. The respective grant numbers are MEA-8104733 and ATM-79-22006.

REFERENCES

ANAND, M. S. & POPE, S. B. 1983 Diffusion behind a line source in grid turbulence. In *Proc. 4th Symp. on Turbulent Shear Flows, Karlsruhe, Germany, 13–16 Sept. 1983.*

ANTONOPOULOS-DOMIS, M. 1981 Large-eddy simulation of a passive scalar in isotropic turbulence. *J. Fluid Mech.* **104**, 55–79.

DURBIN, P. A. 1980 A stochastic model of two-particle dispersion and concentration fluctuations in homogeneous turbulence. *J. Fluid Mech.* **100**, 279–302.

HERRING, J. R., SCHERTZER, D., LESIEUR, M., NEWMAN, G. R., CHOLLET, J. P. & LARCHEVEQUE, M. 1982 A comparative assessment of spectral closures as applied to passive scalar diffusion. *J. Fluid Mech.* **124**, 411–437.

HINZE, J. T. 1975 *Turbulence*, 2nd edn. McGraw-Hill.

KISTLER, A. L. 1954 Ph.D. thesis, The Johns Hopkins University.

LUNDGREN, T. S. 1981 Turbulent pair dispersion and scalar diffusion. *J. Fluid Mech.* **111**, 27–57.

PARANTHOEN, P., PETIT, C. & LECORDIER, J. C. 1982 The effect of the thermal prong–wire interaction on the response of a cold wire in gaseous flows (air, argon and helium). *J. Fluid Mech.* **124**, 457–474.

POPE, S. B. 1981 Transport equation for the joint probability density function of velocity and scalars in turbulent flow. *Phys. Fluids* **24**, 588–596.

POPE, S. B. 1983 Consistent modeling of scalars in turbulent flows. *Phys. Fluids* **26**, 404–408.

SAWFORD, B. L. 1983 The effect of Gaussian particle-pair distribution functions in the statistical theory of concentration fluctuations in homogeneous turbulence. *Q. J. R. Met. Soc.* **109**, 339–354.

SAWFORD, B. L. & HUNT, J. C. R. 1984 Effects of turbulence structure, molecular diffusion and source size on fluctuations of concentration in homogeneous turbulence. Submitted to *J. Fluid Mech.*

SIRIVAT, A. & WARHAFT, Z. 1983 The effect of a passive cross-stream temperature gradient on the evolution of temperature variance and heat flux in grid turbulence. *J. Fluid Mech.* **128**, 323–346.

SREENIVASAN, K. R., TAVOULARIS, S., HENRY, R. & CORRSIN, S. 1980 Temperature fluctuations in grid-generated turbulence. *J. Fluid Mech.* **100**, 597–623.

STAPOUNTZIS, H., SAWFORD, B. L., HUNT, J. C. R. & BRITTER, R. E. 1984 Structure of the temperature field downwind of a line source in grid turbulence. Submitted to *J. Fluid Mech.*

TAYLOR, G. I. 1921 Diffusion by continuous movements. *Proc. Lond. Math. Soc.* **20**, 196–212.

TAYLOR, G. I. 1935 Statistical theory of turbulence. IV – Diffusion in a turbulent air stream. *Proc. R. Soc. Lond.* A **151**, 465–478.

TENNEKES, H. & LUMLEY, J. L. 1972 *A First Course in Turbulence.* MIT Press.

TOWNSEND, A. A. 1954 The diffusion behind a line source in homogeneous turbulence. *Proc. R. Soc. Lond.* A **224**, 487–512.

UBEROI, M. S. & CORRSIN, S. 1953 Diffusion of heat from a line source in isotropic turbulence. *NACA Rep.* 1142.

WARHAFT, Z. 1981 The use of dual heat injection to infer scalar covariance decay in grid turbulence. *J. Fluid Mech.* **104**, 93–109.

WARHAFT, Z. & LUMLEY, J. L. 1978 An experimental study of the decay of temperature fluctuations in grid-generated turbulence. *J. Fluid Mech.* **88**, 659–684.